Journal of Power Sources 196 (2011) 5084–5090

Contents lists available at ScienceDirect

Journal of Power Sources

journal homepage: www.elsevier.com/locate/jpowsour

Performance of (La,Sr)(Co,Fe)O_{3-x} double-layer cathode films for intermediate temperature solid oxide fuel cell

D. Marinha[a,*], J. Hayd[b,c], L. Dessemond[a], E. Ivers-Tiffée[b,c], E. Djurado[a]

[a] Grenoble Institute of Technology/UJF/CNRS (UMR5631), Laboratoire d'Electrochimie et de Physico-Chimie des Matériaux et des Interfaces, 1130 rue de la Piscine, B.P. 75, 38402 St. Martin d'Hères, France
[b] Institut für Werkstoffe der Elektrotechnik (IWE), Karlsruher Institut für Technologie (KIT), 76131 Karlsruhe, Germany
[c] DFG Center for Functional Nanostructures (CFN), Karlsruhe Institute of Technology (KIT), 76131 Karlsruhe, Germany

ARTICLE INFO

Article history:
Received 22 October 2010
Received in revised form 2 December 2010
Accepted 17 January 2011
Available online 25 February 2011

Keywords:
SOFC
Cathode
Double-layer
LSCF
Electrostatic spray deposition
Impedance spectroscopy

ABSTRACT

In this study the performance evaluation of (La,Sr)(Co,Fe)O_{3-x} (LSCF) double-layer films characterized by impedance spectroscopy between 403 and 603 °C to be used for intermediate temperature solid oxide fuel cells (IT-SOFCs) is presented. Two LSCF layers with different microstructures were sequentially deposited onto $Ce_{0.9}Gd_{0.1}O_{1.95}$ (CGO) substrates in a symmetrical fashion. A first layer of $La_{0.6}Sr_{0.4}Co_{0.2}Fe_{0.8}O_{3-x}$ with a thickness of 7 μm and a nano-scaled particle size was deposited by electrostatic spray deposition (ESD) technique. Different deposition conditions were used in preparing the ESD films to evaluate the influence of film morphology on the electrochemical performance. After annealing, a current collector layer of $La_{0.58}Sr_{0.4}Co_{0.2}Fe_{0.8}O_{3-x}$ with ~45 μm in thickness and a larger particle size was deposited by screen printing. Area specific resistances (*ASRs*) were determined from impedance spectroscopy measurements performed in air between 403 and 603 °C, at 25 °C steps. A dependence of electrochemical performance on the morphology of the LSCF layer deposited by ESD was observed. The lowest *ASR*, measured during 130 h of isothermal dwelling at 603 °C, averaged 0.13 Ω cm^2 with negligible variation and is the lowest reported value for this composition, to the best of our knowledge. Reported results assure an excellent suitability of this type of assembly for IT-SOFCs.

1. Introduction

Solid oxide fuel cells (SOFCs) are devices that operate on the basis of thermally activated electrochemical reactions which require a relatively high operating temperature. The components must be chemically compatible to withstand long dwell times at high operation temperatures without reacting with each other, as well as compatible in thermal expansion behavior to endure mechanical stresses during thermal cycling with minimum degradation. Altogether, these factors limit the range of possible practical applications and increase the operation and maintenance costs of SOFCs. The objective is therefore to achieve the maximum performance out of an SOFC operating at the lowest possible temperature. Current research is thereby focused on producing SOFCs to operate between 500 and 700 °C, called intermediate temperature solid oxide fuel cells or IT-SOFCs.

The operation temperature of SOFCs is mainly imposed by the temperature required for the electrolyte to achieve sufficient ionic conductivity. In this sense, significant advances have been made by using thin-film deposition techniques to obtain thinner electrolytes [1,2], thus reducing the electrolyte ohmic resistance. Other significant contributions to the polarization losses originate from the electrochemical reactions at the anode and cathode. Cathode performances have been gradually increasing by using mixed ionic and electronic conductors (MIECs) such as (La,Sr)(Co,Fe)O_{3-x} (LSCF) instead of solely electronic conducting materials like (La,Sr)MnO_{3-x} (LSM). The ability of LSCF to transport oxide ions expands the electrochemically active site from the restricted triple phase boundary of the cathode, electrolyte and gas phase interface to the MIEC material surface. This leads to an improved oxygen reduction reaction (ORR) even at lower temperatures. It is well known that LSCF reacts with yttria-stabilized zirconia (YSZ), the most widely used electrolyte material, resulting in insulating secondary phases across the interface [3]. Ceria-based materials, such as $Ce_{0.9}Gd_{0.1}O_{1.95}$ (CGO), are being evaluated as an alternative to YSZ, as they do not react with LSCF. Currently, the greatest disadvantage of CGO is the electronic leakage in reducing atmospheres which is particularly severe at high temperatures. Nevertheless, it can effectively be used as a buffer layer [4,5] in-between LSCF and YSZ and it remains a good candidate for IT-SOFC, especially in the lower temperature range, where it outperforms YSZ and displays negligible electronic leakage [6]. Recently, losses of a single IT-SOFC consisting of anode,

* Corresponding author. Tel.: +33 4 7682 6684; fax: +33 4 7682 6777.
E-mail address: danielmarinha@gmail.com (D. Marinha).

0378-7753/$ – see front matter © 2011 Elsevier B.V. All rights reserved.
doi:10.1016/j.jpowsour.2011.01.063

electrolyte and cathode were reduced to 0.25 Ω cm^2 at 600 °C using a combination of (La,Sr)CoO_{3-x} (LSC) and CGO as a cathode [7]. Also, fully developed SOFC stacks using LSM and YSZ have been reported to reach 0.26 Ω cm^2 at 800 °C, a performance which was latter obtained at 700 °C when LSM was replaced by LSCF and CGO diffusion barriers were added to avoid the LSCF/YSZ interaction [8].

An overview of the best *ASR* values available in the literature for the $La_{0.6}Sr_{0.4}Co_{0.2}Fe_{0.8}O_{3-x}$ composition results in values ranging from 0.73 Ω cm^2 to 6.94 Ω cm^2 at 600 °C [9–13]. A decrease in *ASR* may be obtained using Co-rich compositions due to increased catalytic and ionic transport properties, with *ASR* values dropping to 0.05 Ω cm^2 [14] and 0.13 Ω cm^2 [15] at 600 °C for $La_{0.4}Sr_{0.6}Co_{0.8}Fe_{0.2}O_{3-x}$ and $La_{0.5}Sr_{0.5}CoO_{3-x}$ compositions, respectively. Nevertheless, the most promising results have been reported for nanostructured $La_{0.6}Sr_{0.4}CoO_{3-x}$ thin-films prepared by metal organic deposition with *ASR* values as low as 0.023 Ω cm^2 at 600 °C [16]. The data scattering observed in comparing results for cathodes with the same chemical composition may be explained, at least in part, by different microstructures of the samples [16,17]. The microstructure of a MIEC electrode is directly related to its performance as a larger surface area facilitates the ORR by increasing the number of active surface sites.

Other microstructural parameters such as film porosity and tortuosity determine how well molecular oxygen can permeate through the film and access the active sites and how well oxide ions can diffuse from the point of the incorporation into the MIEC lattice to the cathode/electrolyte interface. Moreover, adequate current collection must be insured to avoid current constriction issues which decrease the active surface area effectively in use and increase the cathodic polarization resistance [18–21]. In summary, the cathode layer must have a homogeneous microstructure with a large surface area, an adequate porosity, proper lateral grain connectivity for low in-plane resistivity and a good adhesion on the electrolyte. The influence of the current collection becomes increasingly significant if one of these conditions is not met, in which case the number of contact points between the cathode layer and the current collector grid should be maximized by reducing the contact spacing [20]. One way to tackle this issue is by using a double-layered cathode, consisting of a cathode functional layer (CFL) in contact with the electrolyte for the ORR, over which an additional film is deposited to independently act as a current collector layer (CCL). This idea has been previously discussed by Kleitz and Petitbon [22] and has been applied in several other studies [15,23–26]. Still according to Kleitz and Petitbon, the microstructure of the current collector layer should be highly porous, in order to allow easy passage of gas to the active layer underneath, and should have low in-plane resistance to allow homogeneous current distribution.

There are numerous film deposition techniques to prepare SOFC cathode layers. Electrostatic spray deposition (ESD) has the advantage of preparing unique film microstructures, with small particle sizes and large surface areas. ESD technique uses a liquid solution with an adequate mixture of precursor salts which is pumped through a metallic nozzle place beneath a heated substrate. When an electrical field is applied between the nozzle and the substrate, electrohydrodynamic forces cause the solution to break up and form a spray composed of finely dispersed droplets. The spray is directed towards the substrate where due to simultaneous heating and spreading of the droplets, the film is deposited. The microstructure of the final film is highly dependent on the size of the droplets which can be tuned by changing the deposition parameters. More details on the processing technique may be found in previous works [27–29].

The goal of this work is to investigate the influence of the cathode microstructure on the electrochemical properties of LSCF films deposited by ESD onto dense CGO substrates with a $La_{0.58}Sr_{0.4}Co_{0.2}Fe_{0.8}O_{3-x}$ CCL deposited by screen printing.

Table 1
ESD condition for samples 1 and 2.

Sample	T (°C)	d (mm)	q (mL h^{-1})	t (h)
1	350	15	1.6	3
2	400	30	1	4

2. Materials and methods

2.1. Film deposition

The double-layered LSCF films were deposited in a symmetrical fashion on $Ce_{0.9}Gd_{0.1}O_{1.95}$ (Daiichi Kigenso Kagaku Kogyo Co., Ltd., Japan) substrates in a two-step operation, using ESD [29] for the CFL followed by screen printing of the CCL. The CGO disks were ~0.7 mm thick with 25 mm in diameter.

For the ESD process, a precursor salts solution was prepared by weighing and mixing $La(NO_3)_3{\cdot}6H_2O$ (Prolabo, 99.99%, France), $SrCl_2{\cdot}6H_2O$ (Strem Chemicals, 99%, USA), $Co(NO_3)_2{\cdot}6H_2O$ (Sigma–Aldrich, 99.999%, USA) and $Fe(NO_3)_2{\cdot}9H_2O$ (Sigma–Aldrich, 99.99%, USA) salts as to obtain the desired $La_{0.6}Sr_{0.4}Co_{0.2}Fe_{0.8}O_{3-x}$ stoichiometry. Salts were then mixed in absolute ethanol (C_2H_5OH, 99.9%; Prolabo, France) and diethylene glycol monobutyl ether, also known as butyl carbitol ($CH_3(CH_2)_3OCH_2CH_2OCH_2CH_2OH$, 99+%; Acros Organics, Belgium), in a 1:2 volume ratio. The salt concentration in the solution is 0.02 mol L^{-1}.

A total of two samples were prepared and the ESD film deposition conditions concerning the nozzle-to-substrate distances d, solution flow rates q, deposition time t, and substrate temperature T are summarized in Table 1. Deposition temperatures refer to the surface of the substrate facing the solution spray, obtained after temperature calibration with a type K thermocouple. Positive high voltages of approximately 6 kV were used and applied for proper aerosol generation and spray stabilization for each sample. Final film deposition area was ~4.15 cm^2. Samples were fired at 900 °C for 2 h with heating and cooling rates of 3 °C min^{-1} before the application of the CCL.

The $La_{0.58}Sr_{0.4}Co_{0.2}Fe_{0.8}O_{3-x}$ current collector layer was screen printed onto the CFL with an area of 1 cm × 1 cm and was dried at 60 °C for 12 h. The CFL screen printing paste was obtained from the Forschungszentrum Jülich and the particles exhibit a mean diameter of about 0.77 μm. As a high temperature sintering of the current collector would lead to a significant change of the morphology of the CFL, it was used in an unsintered stage and the binder was burned out during the initial heating of the sample for electrochemical characterization.

2.2. Materials and microstructural characterization

Microstructures and elemental analysis of the deposited films were studied using scanning electron microscopy with field-emission gun microscopes ZEISS Ultra 55 (Carl Zeiss NTS GmbH, Germany) coupled with an energy dispersive X-ray (EDX) analyzer and ZEISS 1540XB (Carl Zeiss NTS GmbH, Germany).

2.3. Electrochemical characterization

Electrochemical characterization was performed by means of impedance spectroscopy on a symmetrical cell setup. The active area of the electrostatic spray deposited cathode functional layer was reduced to the size of the current collector layer (1 cm × 1 cm) by cutting it along the border of the current collector layer with a fine diamond cutting disc. The current collector layer was then contacted with a gold mesh (>99.99% Au, 1024 meshes cm^{-2}, 0.06 mm wires) to ensure a homogeneous current distribution over the elec-

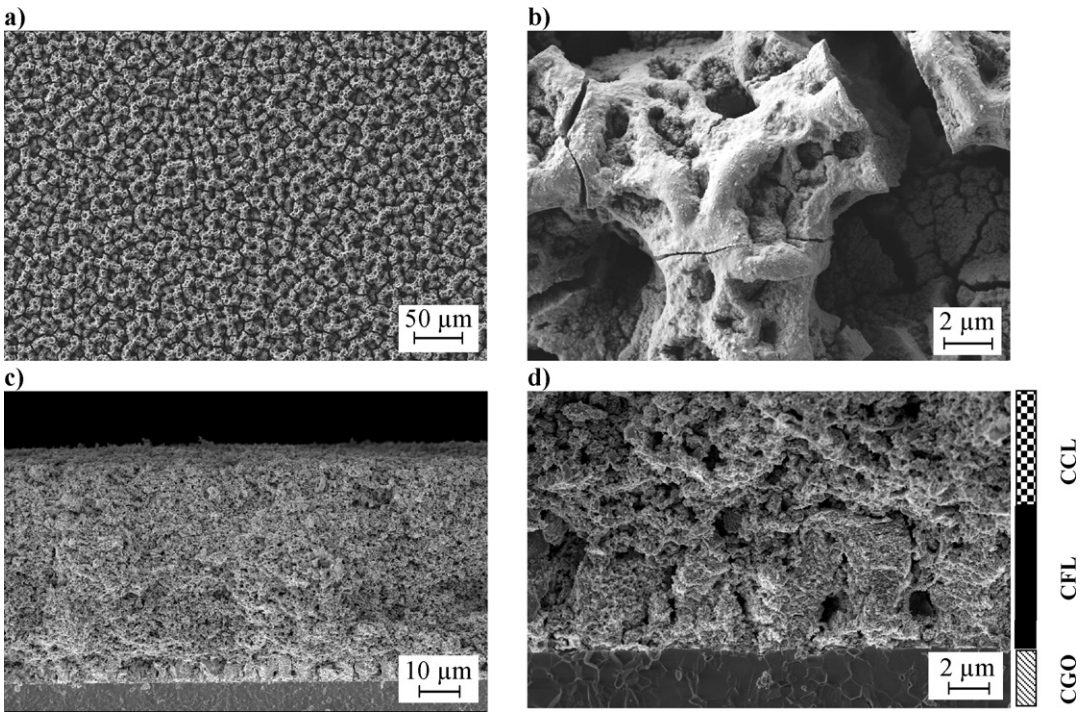

Fig. 1. Surface micrographs of the LSCF layer made by ESD of sample 1 (before testing) (a and b) and cross-section micrographs of the tested sample (with substrate and current collector layer) (c and d).

trode with a low contact resistance [30]. The symmetrical setup was then sandwiched between Al_2O_3 blocks with gas channels, which were pressed together by a weight of 150 g. Electrochemical impedance spectroscopy (EIS) measurements were carried out in stagnant ambient air in temperature steps of 25 °C from 403 to 603 °C using a Solartron 1260 frequency response analyzer operating in a frequency range (f) of $0.05 < f < 10^6$ Hz. The amplitude of the current stimulus was adjusted to a voltage response of 50 mV and the measurements were conducted under open circuit conditions. The impedance data were then analyzed by calculating and analyzing the corresponding distribution function of relaxation times (DRTs) [31] and CNLS fitting with the software package Z-View® (v2.8, Scribner Associates Inc., USA).

3. Results

3.1. Film microstructures

The effect of the different ESD conditions on the morphology of the CFL films is clearly visible in Figs. 1 and 2. The boiling point of the precursor solution was previously determined to be ~270 °C [29]. Sample 1 was deposited using a substrate temperature of 350 °C which allowed the droplets to retain some liquid content upon impacting on the substrate. The rough surface and slight reticulation of the film (Fig. 1a and b) occur due to simultaneous drying and boiling of the liquid droplets as they spread on the surface of the substrate. The cracks appear later during annealing and are caused by retraction and subsequent densification of the film. The thickness of the CFL in sample 1 varied between 7 and 9 μm on both sides, while the CCL thickness averaged 45 μm (Fig. 1c and d).

The deposition conditions for sample 2 were chosen in order to obtain a coral-like microstructure (Fig. 2a and b), which occurs when the liquid droplets in the spray dry due to solvent evaporation during flight towards the substrate [29], resulting in a decrease of droplet size. In order to do so, nozzle-to-substrate distance was increased to provide more time for the droplets to dry in flight, and a smaller flow rate was used resulting in the formation of smaller droplets in the spray [32]. Moreover, the substrate temperature was increased to 400 °C to promote faster droplet drying. Smaller droplets are electrostatically charged and are attracted towards other particles or droplets on the surface of the substrate which have larger curvatures, created by previously deposited droplets due to preferential landing. Successive accumulation of particles makes the superimposed structures visible on the micrographs. Film thickness ranged from 5 and 7 μm for the CFL and an average of 40 μm was determined for the CCL (Fig. 2c and d).

The morphology of the CCL in both samples is highly homogeneous with sub micrometer sized particles and some slightly larger agglomerates. The contact between the CFL and CCL is good in both samples (Figs. 1d and 2d) and no delamination in any of the solid/solid interfaces was observed in any sample, even after being mechanically broken for cross-section observations. The CCL layer sits well separate above the CFL with a less than 1 μm crossover zone, where they are slightly embedded.

The chemical composition of the layers was accessed by EDX (Fig. 3). All peaks in the spectra correspond to the expected layer composition with no foreign elements detected. The average chemical composition was semi-quantified and the results are presented in Table 2, matching with the compositions of the CFL and CCL within the accuracy limits of the method applied.

3.2. Electrochemical characterization

Fig. 4 depicts examples of impedance spectra measured on sample 1 at 603 °C and on sample 2 at 503 °C in form of a Nyquist plot. They were deconvoluted into the ohmic resistance (R_O), the

Table 2
Relative composition of the chemical elements detected by EDX on sample 2.

	La	Sr	Co	Fe
at%	0.55	0.45	0.19	0.81

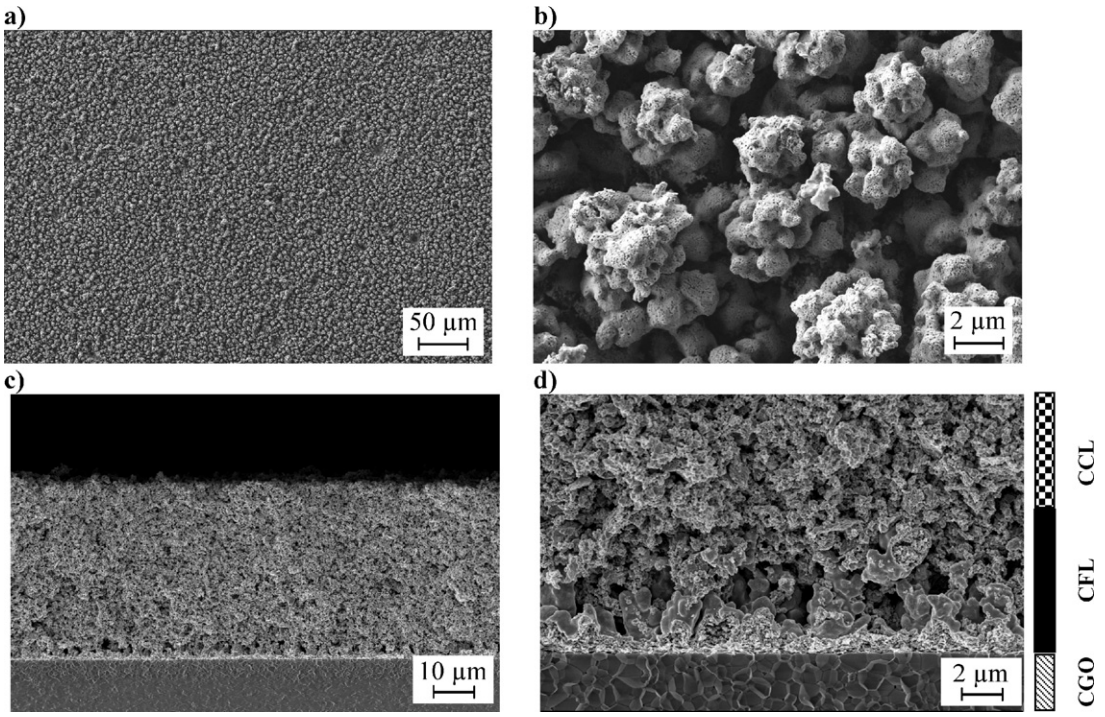

Fig. 2. Surface micrographs of the LSCF layer made by ESD of sample 2 (before testing) (a and b) and cross-section micrographs of the tested sample (with substrate and current collector layer)(c and d).

cathodic polarization losses associated with the electrochemical reaction (*ASR*), and the losses caused by gas diffusion limitations resulting predominantly from the testing setup (ASR_{gas}). The latter only occur at temperatures >550 °C in a detectable magnitude for sample 1 and appear at low frequencies as a separate arc. Since they mainly result from gas diffusion limitations outside the cathode in the flow channels within the contact block, they will not be considered in the following [15].

ASR values derived from the impedance spectroscopy measurements are plotted against temperature in Fig. 5. Samples 1 and 2 exhibit an activation energy of 1.72 eV and 1.36 eV and initial *ASR* values of 0.126 Ω cm^2 and 0.601 Ω cm^2 at 603 °C, respectively. These correspond to the lowest *ASR* values found in the reviewed literature at similar temperatures for the LSCF composition using 20% Co-doping on the B site of the perovskite lattice. Additionally, they compete well even with compositions with higher Co contents, such as $La_{0.4}Sr_{0.6}Co_{0.8}Fe_{0.2}O_{3-x}$ [14] and $La_{0.5}Sr_{0.5}CoO_{3-x}$ [15], only to be outperformed by nanostructured $La_{0.6}Sr_{0.4}CoO_{3-x}$ cathodes [16]. In the latter, the more than five times lower *ASR* values at 500 and 600 °C, 0.25 Ω cm^2 and 0.023 Ω cm^2, respectively, result not only from a different material composition but also from an optimized microstructure, mirroring the potential of a microstructural optimization, in which great progress was achieved for LSCF by applying ESD technique.

The difference of almost fivefold between samples 1 and 2 in this study is explained by the morphological differences of the CFL.

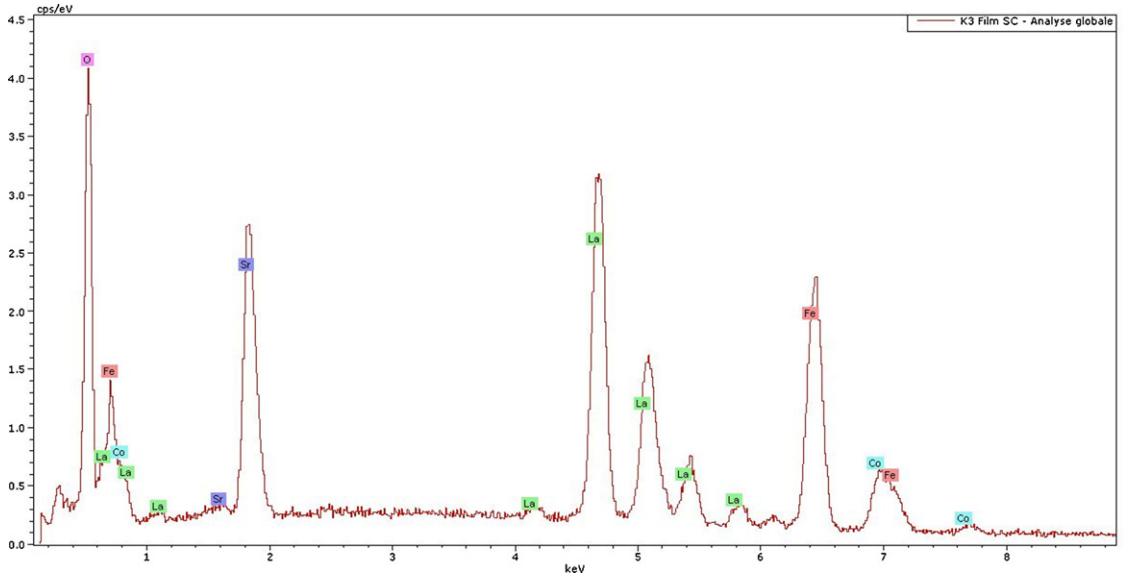

Fig. 3. EDX analysis performed on sample 2.

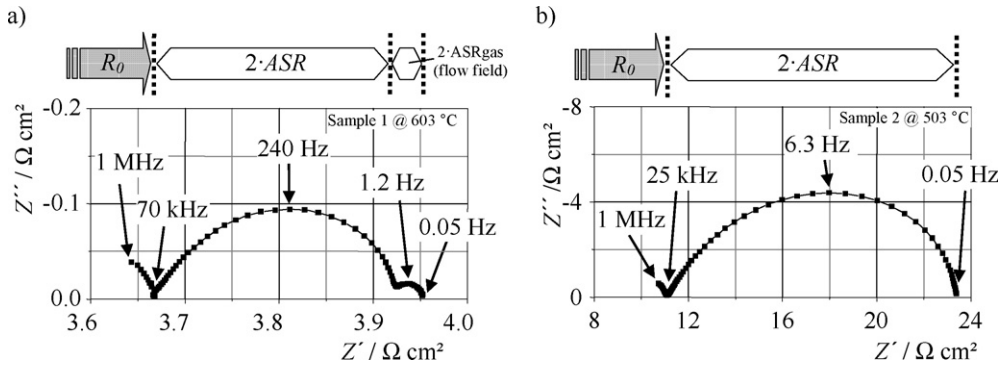

Fig. 4. Examples of impedance spectra of sample 1 at 603 °C (a) and sample 2 at 503 °C (b).

Films prepared by ESD typically show different micrometric-scaled morphological features, such as reticulation and ramification. At smaller length scales, it is possible to observe that the films comprise an inner structure of nano-scaled particles and pores that build up to the microstructural features. Sample 1 has a much more regular structure with maximized surface area and porosity provided by the reticulation and the open pore channels clearly visible on the surface of the film (Fig. 1b). This porosity has ~1 μm in diameter and allows easy access for molecular oxygen gas-phase diffusion and is further increased by the transversal ~1–2 μm gaps resulting from cracking of the CFL film. The beneficial effects of film cracking have already been previously observed [33] and are attributed to the decrease of the resistance associated with the surface exchange, by increasing the total cathode surface area. Furthermore, the gaps allow access of molecular oxygen to the nanostructured microstructure at the interior of the film. As reported by Peters et al., reducing particle size in cathode films to the nanometric range significantly increases the surface area available for the oxygen exchange reaction, resulting in lower polarization resistance values [15,16]. Sample 2 on the other hand, has a large macroscopic porosity due to the spaces between isolated structures. Contrarily to the nano-structured surfaces exposed by film cracking in sample 1, the nano-scaled porosity is observed on the surface of sample 2, only. Therefore the active cathode surface sites available for the oxygen reduction reaction are significantly less than those in sample 1. Furthermore, the increased tortuosity, limited lateral percolation and a smaller total surface area hinder charge transport and result in an additional resistance contribution.

As a measure of stability, impedance measurements were ran during isothermal dwelling at 603 °C for 130 h for sample 1 and 140 h for sample 2 (Fig. 6). *ASR* values of sample 1 remain practically constant, with a maximum variation of 10%, showing the stability of the system at maximum temperature. Sample 2 displays a monotonic decrease from an initial maximum at 0.601 Ω cm^2 to 0.389 Ω cm^2. This decrease is most likely due to further sintering of the CFL microstructure at dwelling temperature improving particle interconnectivity and facilitating the oxide ion diffusion.

A decrease of roughly one order of magnitude of the *ASR* values was observed, compared to LSCF samples with identical compositions prepared similarly by ESD [33]. This enhancement is due to the use of an optimized CCL [15] in a double-layer configuration, which homogenizes the current distribution along the CFL, thus activating a larger volume of the cathode and avoiding any current constriction issues.

The literature shows a large dispersion of activation energy values of LSCF films deposited on CGO substrates, ranging from 1.23 to 1.69 eV [11–13,34–39]. Samples 1 and 2 are near the higher and lower limits of this dispersion and speak for the relevance of morphology on cathode performance. An even greater dispersion of activation energy values corresponding to the elementary processes of surface exchange (1.09–2.5 eV) [40,41] and the oxygen bulk diffusion (0.64–1.93) [41,42] can be found. Available data are therefore insufficient for an accurate analysis regarding the dominant mechanism for the cathode reaction in this type of layers.

A definite conclusion as to whether or not the current collector layer has an influence on the electrochemical reaction cannot be drawn at this point. Further measurements are necessary to eluci-

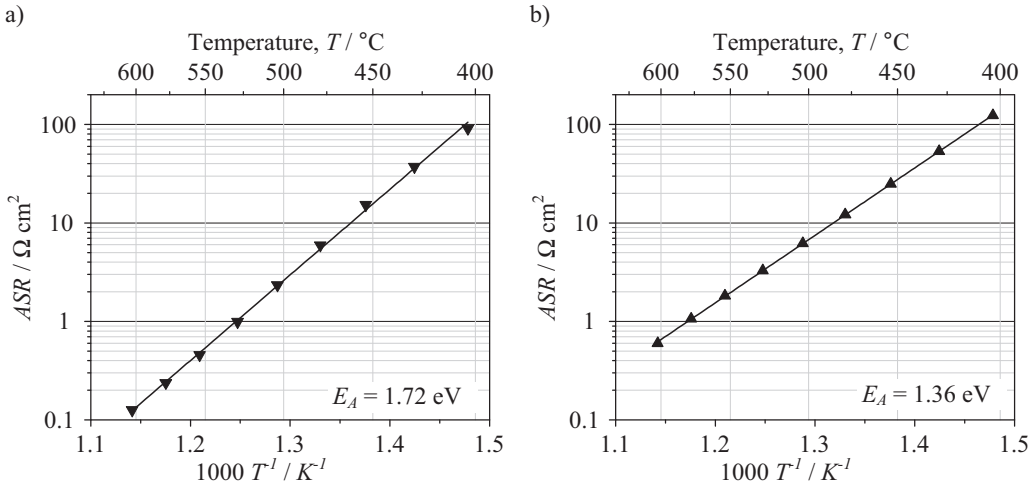

Fig. 5. *ASR* vs. temperature for sample 1 (a) and sample 2 (b).

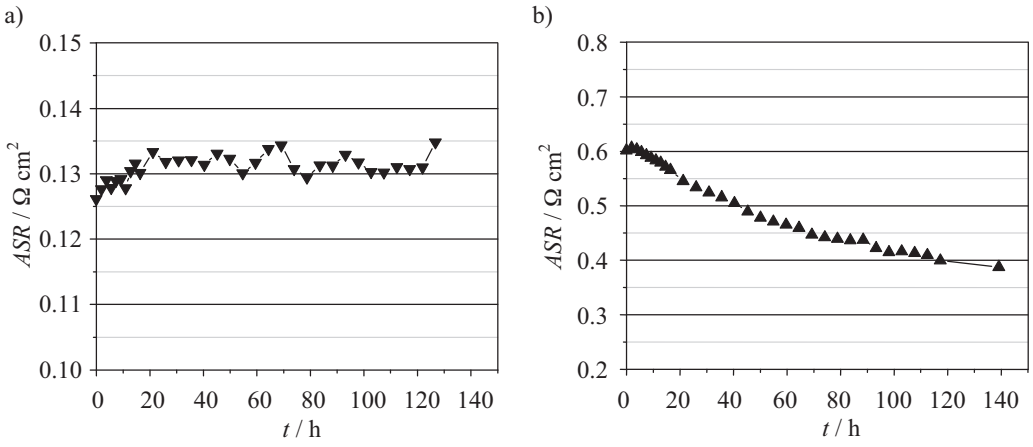

Fig. 6. ASR values for sample 1 (a) measured at 603 °C for 130 h, and sample 2 (b) measured at 603 °C for 140 h.

date this question. Another approach to investigate the influence of the CCL on the electrochemistry is to determine whether the penetration depth of the cathodic reaction (δ) exceeds the thickness of the CFL, in which case the CCL is most likely active to a certain extent. This can for example be done as described by Adler et al. [16,17] by 1-D modeling. Nevertheless, it is worth mentioning that the application of such a modeling approach is necessarily vague in this case, due to the microstructural complexity of the cathode films presented here. Therefore, only a rough estimate can be given. According to Adler et al. [16,17] the penetration depth of the cathodic reaction for a MIEC cathode can be calculated by the following equation:

$$\delta = \sqrt{\frac{(1-\varepsilon)}{\tau} \cdot \frac{L_c}{a}} \quad (1)$$

where ε is the porosity of the cathode, τ is the tortuosity, a is the volume specific surface area, and L_c is the characteristic thickness. L_c is calculated by the ratio of the oxygen self-diffusion coefficient D_O and the oxygen surface exchange coefficient k_O [43] and can also be expressed by the ratio of the chemical diffusion and the surface exchange coefficients D_{chem} and k_{chem} obtained by a conductivity relaxation experiment [44].

$$L_c = \frac{D_O}{k_O} \approx \frac{D_{chem}}{k_{chem}} \quad (2)$$

Following the example in [17] and assuming $\varepsilon = 0.5$, $\tau = 1$, $a = 3\ \mu m^{-1}$ (corresponding to a particle diameter of 1 μm) in combination with the material related data for $La_{0.6}Sr_{0.4}Co_{0.2}Fe_{0.8}O_{3-x}$ from [45] the penetration depth of the cathodic reaction calculates to ~2.6 μm at 600 °C (using extrapolated data). Again, as the active surface area can easily differ by a factor of 2 or more and as a tortuosity of $\tau = 1$ is very low (values of 1.5–2.5 are more realistic [16,46]), not to mention the large scatter in data for the k and D values, the derived value serves as a rough estimate. Therefore, although a possible influence of the CCL cannot be completely ruled out at this point, it is safe to say that the major part of the oxygen reduction reaction takes place within the CFL of 5–9 μm thickness, which consequently dominates the overall cathodic electrochemical characteristic.

4. Conclusions

In this work, double-layered LSCF-based cathode films were prepared consisting of a microstructurally complex cathode functional layer with microstructural features in the nanometer range and an optimized current collection layer. This strategy was successful in significantly lowering the *ASR* values from 0.82 Ω cm², as reported in a previous study [33], to 0.13 Ω cm² at 600 °C in air compared to results of LSCF cathodes with similar chemical composition. This improvement is attributed to the addition of a CCL, which improves the current distribution within the CFL volume, thus maximizing the active cathode surface area while avoiding current constriction issues. The influence of the CCL on the electrochemistry should be negligible, as the penetration depth of the cathodic reaction is expected to be smaller than the thickness of the CFL.

Encouraging results were obtained for LSCF double-layer cathodes indicating that further improvement may be achieved by optimizing the microstructure of the assembly. Specifically, a systematic variation of the thickness and morphology of the CFL, obtained by varying the ESD conditions, is expected to give conclusive results.

References

[1] Y.S. Xie, R. Neagu, C.S. Hsu, X.G. Zhang, C. Deces-Petit, W. Qu, R. Hui, S. Yick, M. Robertson, R. Maric, D. Ghosh, J. Fuel Cell Sci. Technol. 7 (2010) 021006–021007.
[2] F. Han, A. Leonide, T. van Gestel, H.P. Buchkremer, Proceedings of the 9th European Solid Oxide Fuel Cell Forum, Lucerne, Switzerland, 2010, pp. 1–9.
[3] O. Yamamoto, Y. Takeda, R. Kanno, M. Noda, Solid State Ionics 22 (1987) 241–246.
[4] J. Pena-Martinez, D. Marrero-Lopez, C. Sanchez-Bautista, A.J. Dos Santos-Garcia, J.C. Ruiz-Morales, J. Canales-Vazquez, P. Nunez, Bol. Soc. Esp. Ceram. V 49 (2010) 15–22.
[5] H.R. Rim, S.K. Jeung, E. Jung, J.S. Lee, Mater. Chem. Phys. 52 (1998) 54–59.
[6] B.C.H. Steele, Solid State Ionics 129 (2000) 95–110.
[7] B. Rietveld, F. van Berkel, Y. Zhang-Steenwinkel, E. Bouyer, J. Irvine, M. Menon, L. Niewolak, S. Gross, A. Heel, P. Holtappels, S. Modena, ECS Trans. 25 (2009) 29–34.
[8] R. Steinberger-Wilckens, O. Bucheli, L.G.J. de Haart, A. Hagen, J. Kiviaho, J. Larsen, S. Pyke, J. Sfeir, A. Tietz, M. Zahid, ECS Trans. 25 (2009) 43–56.
[9] A. Mai, V.A.C. Haanappel, S. Uhlenbruck, F. Tietz, D. Stover, Solid State Ionics 176 (2005) 1341–1350.
[10] A. Esquirol, N.P. Brandon, J.A. Kilner, M. Mogensen, J. Electrochem. Soc. 151 (2004) A1847–A1855.
[11] Y.J. Leng, S.H. Chan, Q.L. Liu, Int. J. Hydrogen Energy 33 (2008) 3808–3817.
[12] D. Beckel, U.P. Muecke, T. Gyger, G. Florey, A. Infortuna, L.J. Gauckler, Solid State Ionics 178 (2007) 407–415.
[13] C.S. Hsu, B.H. Hwang, J. Electrochem. Soc. 153 (2006) A1478–A1483.
[14] L. Baque, A. Caneiro, M.S. Moreno, A. Serquis, Electrochem. Commun. 10 (2008) 1905–1908.
[15] C. Peters, A. Weber, E. Ivers-Tiffée, J. Electrochem. Soc. 155 (2008) B730–B737.
[16] J. Hayd, U. Guntow, E. Ivers-Tiffée, ECS Trans. 28 (2010) 3–15.
[17] S.B. Adler, J.A. Lane, B.C.H. Steele, J. Electrochem. Soc. 143 (1996) 3554–3564.
[18] K. Sasaki, J.P. Wurth, R. Gschwend, M. Godickemeier, L.J. Gauckler, J. Electrochem. Soc. 143 (1996) 530–543.
[19] S. Koch, P.V. Hendriksen, Solid State Ionics 168 (2004) 1–11.
[20] S.P. Jiang, J.G. Love, L. Apateanu, Solid State Ionics 160 (2003) 15–26.
[21] Y. Takeda, R. Kanno, M. Noda, Y. Tomida, O. Yamamoto, J. Electrochem. Soc. 134 (1987) 2656–2661.
[22] M. Kleitz, F. Petitbon, Solid State Ionics 92 (1996) 65–74.
[23] M.J. Jorgensen, S. Primdahl, C. Bagger, M. Mogensen, Solid State Ionics 139 (2001) 1–11.

[24] Y. Tao, H. Nishino, S. Ashidate, H. Kokubo, M. Watanabe, H. Uchida, Electrochim. Acta 54 (2009) 3309–3315.
[25] C.S. Hsu, B.H. Hwang, Y. Xie, X. Zhang, J. Electrochem. Soc. 155 (2008) B1240–B1243.
[26] H.Y. Jung, W.S. Kim, S.H. Choi, H.C. Kim, J. Kim, H.W. Lee, J.H. Lee, J. Power Sources 155 (2006) 145–151.
[27] R. Neagu, D. Perednis, A. Princivalle, E. Djurado, Solid State Ionics 177 (2006) 1981–1984.
[28] R. Neagu, D. Perednis, A.S. Princivalle, E. Djurado, Chem. Mater. 17 (2005) 902–910.
[29] D. Marinha, C. Rossignol, E. Djurado, J. Solid State Chem. 182 (2009) 1742–1748.
[30] A. Weber, A.C. Müller, D. Herbstritt, E. Ivers-Tiffée, in: H. Yokokawa, S.C. Singhal (Eds.), Seventh International Symposium on Solid Oxide Fuel Cells (SOFC-VII), 2001, pp. 952–962.
[31] H. Schichlein, A.C. Muller, M. Voigts, A. Krugel, E. Ivers-Tiffée, J. Appl. Electrochem. 32 (2002) 875–882.
[32] A.M. Gañan-Calvo, J. Davila, A. Barrero, J. Aerosol Sci. 28 (1997) 249–275.
[33] D. Marinha, L. Dessemond, E. Djurado, ECS Trans. 28 (2010) 93–103.
[34] E.P. Murray, M.J. Sever, S.A. Barnett, Solid State Ionics 148 (2002) 27–34.
[35] W.I. Zhou, Z.P. Shao, R. Ran, H.X. Gu, W.Q. Jin, N.P. Xu, J. Am. Ceram. Soc. 91 (2008) 1155–1162.
[36] X.Y. Lou, S.Z. Wang, Z. Liu, L. Yang, M.L. Liu, Solid State Ionics 180 (2009) 1285–1289.
[37] H.J. Hwang, M.B. Ji-Woong, L.A. Seunghun, E.A. Lee, J. Power Sources 145 (2005) 243–248.
[38] V.C. Kournoutis, F. Tietz, S. Bebelis, Fuel Cells 9 (2009) 852–860.
[39] A. Leonide, Y. Apel, E. Ivers-Tiffée, ECS Trans. 19 (2009) 81–109.
[40] S.J. Xu, W.J. Thomson, Chem. Eng. Sci. 54 (1999) 3839–3850.
[41] B.C.H. Steele, J.M. Bae, Solid State Ionics 106 (1998) 255–261.
[42] B.T. Dalslet, M. Sogaard, P.V. Hendriksen, Solid State Ionics 180 (2009) 1050–1060.
[43] H.J.M. Bouwmeester, H. Kruidhof, A.J. Burggraaf, Solid State Ionics 72 (1994) 185–194.
[44] J.E. tenElshof, M.H.R. Lankhorst, H.J.M. Bouwmeester, J. Electrochem. Soc. 144 (1997) 1060–1067.
[45] H.J.M. Bouwmeester, M.W. Den Otter, B.A. Boukamp, J. Solid State Electrochem. 8 (2004) 599–605.
[46] S.B. Adler, Solid State Ionics 111 (1998) 125–134.